Journal of Engineering Research xxx (xxxx) xxx

Contents lists available at ScienceDirect

Journal of Engineering Research

journal homepage: www.journals.elsevier.com/journal-of-engineering-research

Prabhakar fractional simulations for natural convective hybrid nanofluid mixed with *Cu* and Al_2O_3 nanoparticles flowing through a channel

Ali Raza [a,b], Rifaqat Ali [c], Ali Hasan Ali [d,e,f,*], Suleman H. Alfalqi [c], Kalsoom Chishti [b]

[a] Department of Mathematics, University of Engineering and Technology, Lahore 54890, Pakistan
[b] Department of Mathematics, Minhaj University, Lahore 54770, Pakistan
[c] Department of Mathematics, College of Scinece and Arts, Muhayil, King Khalid University, Abha, Saudi Arabia
[d] Institute of the Mathematics, University of Debrecen, Pf. 400, H-4002 Debrecen, Hungary
[e] Department of Mathematics, College of Education for Pure Sciences, University of Basrah, Basrah 61001, Iraq
[f] College of Engineering Technology, National University of Science and Technology, Dhi Qar 64001, Iraq

ARTICLE INFO

Keywords:
Water
Nanofluid
Newtonian heating
Parallel plates
Mittage-Leffler function

ABSTRACT

This study seeks to investigate the heat transfer analysis of hybrid nanofluids containing fractionalized water and kerosene oil, which flow through a vertical channel via convection. To represent the problem in terms of fractional partial differential equations, we utilized the Prabhakar time-fractional derivative, a recent advancement in the concept of fractional derivatives. The governing equations were then solved using physical initial and boundary conditions that include momentum, concentration, and energy equations. Stehfest and Tzou's Laplace inversion techniques are used to provide semi-analytical solutions for governed equations, such as temperature, concentration, and momentum profiles, and we applied the fractional Laplace transformation to find solutions in the transform domain. Furthermore, the resultant solutions in tabular form are also derived using Tzou and Stehfest's numerical methods for Laplace inversion to ensure the accuracy of our findings. According to our research, an increase in volumetric fraction causes a reduction in fluid velocity. Due to the physical properties of the investigated nanoparticles, the water-based hybrid nanofluid has a bigger effect on the temperature and momentum profile than the kerosene oil-based hybrid nanofluid.

1. Introduction

There are numerous industrial uses for channel flow, with heat transfers in nuclear power plants also biochemical reactors in enhancement sector. However, different applied curiosity phenomena could be viewed through two-sided flows through Newtonian actions in twain operations. The continuous fluid phase shows non-Newtonian flow structures in numerous related contributions. Several instances exist in the biological, biomedical, and food-preserving areas [1]. Zheng et al. [2] studied the influence of the vortex-producer system in different fluids also the thermal conversion of HNFs in a channel. D'D'D'Ippolito et al. [3] considered the confrontation in the flow in an open channel due to vegetation in their study. Firstly, Choi [4] used the term Nanofluids are supposed to be identical in substantial investigations due to their heat transmission expansion application. According to a few recent studies, NFs have better thermal transmission capabilities than traditional fluids. Therefore, using NFs to convert common fluids is feasible. Many investigators are drawn to the examination of NFs because of their highly developed heat skill. They participate actively in industries like nuclear reactors, biomedicine, electronics, food, and transportation. Nanoparticles (NPs) are small in size, and by being added to base fluids, they improve the conductivity of such fluids. The structure of NPs contains nitride, carbon tubes, metal oxide, carbide, and metals [5]. The characterizations of a micropolar heat flux model based on magnesium oxide are discussed in [6]. The influence of NPs combined ratio, and the thermal and diffusion profile on the heat conductivity of HNFs, was recognized by Wole-Osho et al. [7]. The laminar NPs with thermal transfer, invoking convection strength in the existence of noncircular channels, were explored by Haque et al. [8]. Khashi'ie et al. [9] considered HNFs in view of melting thermal transmission. They considered a rotating surface. Goldanlou et al. [10] presented a thermal transfer pipe arranged by turbulators to transfer HNFs through a vertical wall. The improvement of the novel relations and the thermal transfer of

* Corresponding author at: Institute of the Mathematics, University of Debrecen, Pf. 400, H-4002 Debrecen, Hungary.
E-mail addresses: rrafat@kku.edu.sa (A. Raza), aliraza.math@mul.edu.pk (R. Ali), ali.hasan@science.unideb.hu (A.H. Ali), salfalqi@kku.edu.sa (S.H. Alfalqi), kalsoom.math@mul.edu.pk (K. Chishti).

https://doi.org/10.1016/j.jer.2023.08.027
Received 17 April 2023; Received in revised form 22 July 2023; Accepted 31 August 2023
Available online 2 September 2023

Nomenclature

Symbol	quantity, Unit
T_d	ambient temperature, (K)
θ	angle of magnetic inclination, $(-)$
μ_{nf}	dynamic viscosity, (Kg/ms)
W	fluid velocity, (m/s)
g	gravity acceleration, (m/s^2)
Gr	heat Grashof number, $(-)$
M	magnetic field, $(-)$
B_o	magnetic field strength, (Kg/s^2)
Gm	mass Grashof number, $(-)$
ρ_{nf}	nanofluid density, (Kg/m^3)
Pr_{eff}	Prandtl number, $(-)$
α, β, γ	Prabhakar Fractional parameters, $(-)$
Sc	Schmidt number, $(-)$
C_p	specific heat at constant pressure, (J/kgK)
k_{nf}	thermal conductivity of the nanofluid, (W/mk)
β_T	thermal expansion coefficient, $(1/k)$
t	times, (s)
T_w	wall temperature, (K)

the stormy NPs was discussed in [11]. Raza et al. [12] utilized the Prabhakar fractional approach to investigate the thermal intensivity of CMC base hybrid nanofluid with different type of nanoparticles. Ahmad et al. [13] have also used the fractional approach for the solution of the bioconvective thermal transport type nofluid with viscous dissipation. In [14] authors utilized the prabhakar fractional approach with slip conditions a hybrid type nanofluid flowing through a pored channel. The horizontal cylinder with different forms NPs, resulting in convection thermal transmission exhibition of HNFs, was discussed in [15]. The plate in the energy transfer hydrothermal demonstration of HNFs was discussed in [16]. Izadi et al. [17] deliberated the 3-D hole and the characteristics of porous solids on the usual transitory convection of the thermal transmission of NFs.

Regarding the HNF, a mixture of two different nano-sized atoms in base fluids that affect convective thermal transfer, one can follow prior studies by many researchers. Waini et al. [18] investigated the specific form of fully developed flowing in an absorbent medium using HNFs. Pandya et al. [19] inspected the computational flow model established to utilize the thermal presentation of an axial lined thermal duct used on MWCNT+CeO2/H2O HNFs. Using only a permeable normal, Babazadeh et al. [20] examined the HNF of normal convection transportation in the case of a superficially applied magnetic influence. They represented it with control loudness using a static element technique. The research of HNF n on system presentation was considered in Asadi et al. [21]. Ikram et al. [22] used a new fractional systematic model that extracts NFs to investigate clay NPs in various fluids. The study by Huminic et al. [23] looked at possible thermal constructions that may be envisaged at various boundary conditions and physical scenarios. However, it was limited to an examination of the NF and HNF entropy generation. In their investigation, Nadeem et al. [24] examined the base fluid culmination with a stretching surface. The examination estimates the effect of the conditions of the HNFs. Further the recent work on different fractional schemes can be seen in [25–28].

Fractional calculus (FC), recently gaining popularity in various academic domains, can define the memory impact of various physical procedures. Numerous scientific disciplines, including viscoelasticity, electrochemistry, mechanics, biophysics, engineering, electrical rheology, mechatronics, and biology, now make excellent use of FC [29]. Numerous mathematical operations, such as various fractional derivatives, are examples. These include Hadamard, Marchand, Liouville, Riemann-Liouville, Grünwald-Letnikov, Caputo Fabrizio, Riesz,

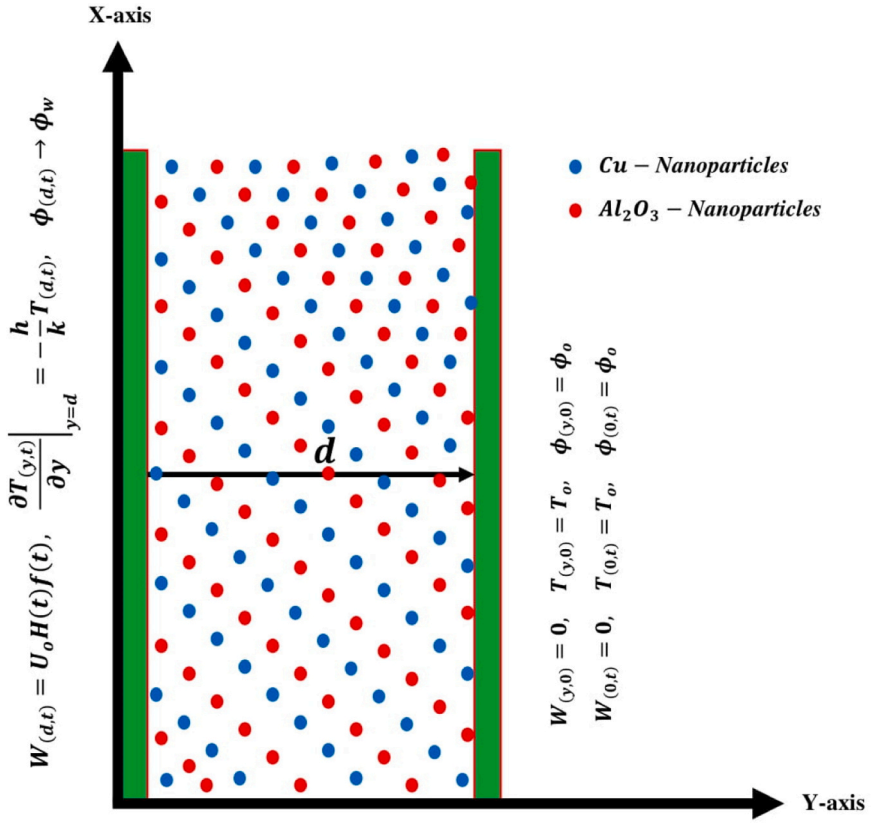

Fig. 1. Flow geometry.

Table 1
Exemplary for thermophysical characteristics of regular and hybrid nanofluid quantities.

Thermal constraints	Regular Nanofluid	Hybrid Nanofluid
Density	$\rho_f = \frac{\rho_{nf}}{(1-\varphi)+\varphi\frac{\rho_s}{\rho_s}}$	$\rho_f = \frac{\rho_{hnf}}{\left((1-\varphi_2)\left((1-\varphi_1)+\varphi_1\frac{\rho_{s1}}{\rho_f}\right)+\varphi_2\rho_{s2}\right)}$
Dynamic Viscosity	$\mu_f = \mu_{nf}(1-\varphi)^{2.5}$	$\mu_f = \mu_{hnf}(1-\varphi_1)^{2.5}(1-\varphi_2)^{2.5}$
Electrical conductivity	$\sigma_f = \frac{\sigma_{nf}}{\left(1+\frac{3\left(\frac{\sigma_s}{\sigma_f}-1\right)\varphi}{\left(\frac{\sigma_s}{\sigma_f}+2\right)-\left(\frac{\sigma_s}{\sigma_f}-1\right)\varphi}\right)}$	$\sigma_{bf} = \frac{\sigma_{hnf}}{\left(1+\frac{3\varphi(\varphi_1\sigma_1+\varphi_2\sigma_2-\sigma_{bf}(\varphi_1+\varphi_2))}{(\varphi_1\sigma_1+\varphi_2\sigma_2+2\varphi\sigma_{bf}-\varphi\sigma_{bf}(\varphi_1\sigma_1+\varphi_2\sigma_2-\sigma_{bf}(\varphi_1+\varphi_2)))}\right)}$
Thermal conductivity	$\frac{k_{nf}}{k_f} = \left(\frac{k_s+(n-1)k_f-(n-1)(k_f-k_s)\varphi}{k_s+(n-1)k_f+(k_f-k_s)\varphi}\right)$	$\frac{k_{hnf}}{k_{bf}} = \left(\frac{k_{s2}+(n-1)k_{bf}-(n-1)(k_{bf}-k_{s2})\varphi_2}{k_{s2}+(n-1)k_{bf}+(k_{bf}-k_{s2})\varphi_2}\right)$
Heat capacitance	$(\rho C_p)_f = \frac{(\rho C_p)_{nf}}{(1-\varphi)+\varphi\frac{(\rho C_p)_s}{(\rho C_p)_f}}$	$(1-\varphi_2)\left((1-\varphi_1)+\varphi_1\frac{(\rho C_p)_{s1}}{(\rho C_p)_f}\right)+\varphi_2(\rho C_p)_{s2} = \frac{(\rho C_p)_{hnf}}{(\rho C_p)_s}$
Thermal Expansion Coefficient	$(\rho\beta)_f = \frac{(\rho\beta)_{nf}}{(1-\varphi)+\varphi\frac{(\rho\beta)_s}{(\rho\beta)_f}}$	$(\rho\beta)_f = \frac{(\rho\beta)_{hnf}}{(1-\varphi_2)\left((1-\varphi_1)+\varphi_1\frac{(\rho\beta)_{s1}}{(\rho\beta)_{f1}}\right)+\varphi_2(\rho\beta)_{s2}}$

Leibnitz, Atangana-Baleanu, Caputo, Prabhakar operator, etc. Essential derivatives are generalizations of ordinary derivatives. According to Caputo, the Fourier Law has only recently been used to analyze issues with energy transfer. The Caputo fractional operator is applied to originate the fractional model for the heat equation [30–32]. Hristov [33] used the integral-balance approach to derive closed-form computational form solutions to the diffusion model issue via the Kirchhoff transformation. The essential features of the Prabhakar functions [34] also the Mittag-Leffler with three-parameter functions supplied through Gara-Garrappa [35]. The relevancy of Prabhakar's functions in analyzing the parting dielectric properties for chaotic materials and mixed schemes that demonstrate non-locality and non-linearity at the equivalent time is clearly identified. Giusti also Colombaro [36] proposed a linearly viscoelastic version of the model due to the Prabhakar fractional derivatives.

In this research, water and kerosene oil-based hybrid nanofluids are used to study free convection flows of Prabhakar's type fractionalized heat transfer in a vertical channel. The generalized thermal transfer non-integer governed equations serve as the foundation for this mathematical model. In order to fully understand the memory impact, we created a time-fractional Prabhakar operator-based fractional model. The dimensionless thermal, concentration, and temperature problems are resolved by the Laplace method. Tabular analysis is used to assess the reliability of the solutions that are produced. Tzou and Stehfest's numerical techniques are used in the Laplace inversion. On a visual plot, the impacts of various restrictions on various nanoparticles are evaluated.

2. Problem description

Consider a compact, unsteady, free convective hybrid nanofluid that passes through the trail of two parallel plates possessing mass diffusion and temperature incline traits. The considered hybrid nanofluid is mixed with copper $(Cu)$and aluminum oxide (Al_2O_3) nanoparticles with water (H_2O) and kerosene oil as base fluid. The two plates are fixed in xy-plane with a distance d parallel to the x-axis also vertical to the y-axis, as shown in Fig. 1. Initially, the whole system with fluid and its corresponding constraints is in equilibrium. For time $t > 0^+$, one plate starts to move under the applied time-dependent shear stress. The nanofluid begins to move between the poured plates as a result of oscillations and the surrounding temperature. A constant magnetic field through an inclination angle$\vartheta$is functional to the flowing fluid. The following assumptions are made for this flow model.

- The parallel plates is infinite in length through distance d.
- The decanted plates are perpendicular to the y-axis also concerned with in the x-direction.
- At $t \le 0$, together temperature also concentration have continuous values as $T_o also \phi_o$ correspondingly.
- A mixed hybrid nanofluid with dissimilar nanoparticles flow in the x direction.
- The continuous magnetic field of power B_o is applied to flowing fluid.
- With the help of the Boussinseq's approximation [37] and Roseland approximations [38], the governed partial differential equations could be expressed by the way of [39]

$$\rho_{hbnf}\frac{\partial W_{(y,t)}}{\partial t} = \mu_{hbnf}\left(1+\lambda_2\frac{\partial}{\partial t}\right)\frac{\partial^2 W_{(y,t)}}{\partial y^2} - \left(\sigma_{nf}B_o^2\sin(\theta)+\frac{\mu_{hbnf}}{K}\right)W_{(y,t)} + g(\rho\beta_T)_{hbnf}\left(T_{(y,t)}-T_o\right)+g(\rho\beta_C)_{hbnf}\left(\phi_{(y,t)}-\phi_o\right) \tag{1}$$

$$\left(\rho C_p\right)_{hbnf}\frac{\partial T_{(y,t)}}{\partial t} = -\frac{\partial q_{(y,t)}}{\partial y}, q_{(y,t)} = -k_{nf}\frac{\partial T_{(y,t)}}{\partial y} \tag{2}$$

$$\frac{\partial \phi_{(y,t)}}{\partial t} = -\frac{\partial J_{(y,t)}}{\partial y}, J_{(y,t)} = -D\frac{\partial \phi_{(y,t)}}{\partial y} \tag{3}$$

where a list of all the conditions and variables may be found in the nomenclature section. The following are the constant conditions for the governed equations.

$$W_{(y,0)} = 0, T_{(y,0)} = T_o, \phi_{(y,0)} = \phi_o; \forall y \ge 0 \tag{4}$$

$$W_{(0,t)} = 0, T_{(0,t)} = T_o, \phi_{(0,t)} = \phi_o; y = 0 \tag{5}$$

$$W_{(d,t)} = U_o H(t) f(t), \left.\frac{\partial T_{(y,t)}}{\partial y}\right|_{y=d} = -\frac{h}{k}T_{(d,t)}, \phi_{(d,t)} \to \phi_w; t > 0 \tag{6}$$

Now the subsequent dimensionless factors have been incorporated, the linked conducted factors may not be dimensionalized in order to examine the impact of all inducing parameters

$$W^* = \frac{W}{U_o}, t^* = \frac{U_o t}{d}, y^* = \frac{y}{d}, T^* = \frac{T_{(y,t)}-T_o}{T_w-T_o}, \delta^* = \delta_o$$

$$\phi^* = \frac{\phi_{(y,t)}-\phi_o}{\phi_w-\phi_o}, Sc = \frac{dU_o}{D}, Ra = \frac{\rho d U_o}{\mu}, M = \frac{\sigma^* dB_o^2}{\rho U_o}, Gr = \frac{g\beta_T d(T_w-T_o)}{U_o^2}$$

$$K_{eff} = \frac{\nu}{K^* U_o^2}, \lambda = \frac{\lambda_2 U_o}{d}, Pe = \frac{\left(\rho C_p\right)_f d U_o}{k_f} \quad Gm = \frac{g\beta_C d(\phi_w-\phi_o)d}{U_o^2}$$

Table 2
The thermal properties of common fluids also nanoparticles.

Material	H_2O	Kerosene Oil	Al_2O_3	Cu
$\rho(kg/m^3)$	997.1	783	3970	8933
$C_p(J/kg\ K)$	4179	2090	765	385
$k(W/m\ K)$	0.613	0.145	40	401
$\beta_T \times 10^{-5}(K^{-1})$	21	99	1.67	1.67
$\beta_C \times 10^{-5}(K^{-1})$	298.2	117	4.05	3.05
Pr	6.2	23	-	-

It can be obtained by modifying the aforementioned dimensionless variables in the regulated equations and conditions (1)–(6) while ignoring the "* " symbols. We get as follows

$$\frac{\partial W_{(y,t)}}{\partial t} = a_7 \frac{\partial^2 W_{(y,t)}}{\partial y^2} + a_7 \lambda \frac{\partial^3 W_{(y,t)}}{\partial t \partial y^2} - \left(a_8 M \sin(\theta) + a_5 K_{eff}\right) W_{(y,t)} + a_9 \quad Gr \quad T_{(y,t)} + a_{10} \quad Gm \tag{7}$$

$$b_o \frac{\partial T_{(y,t)}}{\partial t} = -\frac{\partial \delta_{(y,t)}}{\partial y}, \quad \delta_{(y,t)} = -\frac{\partial T_{(y,t)}}{\partial y} \tag{8}$$

$$b_1 \frac{\partial \phi_{(y,t)}}{\partial t} = -\frac{\partial J_{(y,t)}}{\partial y}, J_{(y,t)} = -\frac{\partial \phi_{(y,t)}}{\partial y} \tag{9}$$

Through undeviating dimensionless conditions

$$W_{(y,0)} = 0, T_{(y,0)} = 0, \phi_{(y,0)} = 0; \forall y \geq 0 \tag{10}$$

$$W_{(0,t)} = 0, T_{(0,t)} = 0, \phi_{(0,t)} = 0; t > 0 \tag{11}$$

$$W_{(1,t)} = H(t) f(t), \left.\frac{\partial T_{(y,t)}}{\partial y}\right|_{y=d} = -\left(1 + T_{(1,t)}\right), C_{(1,t)} = 1; t > 0 \tag{12}$$

where M, Gr, Pr, Pe, K, Gm, Sc respectively, stand in for the magnetic parameter, heat Grashof number, Prandtl number, Peclet number, porosity parameter, mass Grashof number, and Schmidt number. Tables 1 and 2 provide a list of the base material, the proposed nanofluid model, and the thermal properties of solid nanoparticles.

$$a_1 = (1-\varphi) + \frac{\varphi \rho_s}{\rho_f}, a_2 = 1 + \frac{3\left(\frac{\sigma_s}{\sigma_f} - 1\right)\varphi}{\left(\frac{\sigma_s}{\sigma_f} + 2\right) - \left(\frac{\sigma_s}{\sigma_f} - 1\right)\varphi}, a_3 = (1-\varphi) + \frac{\varphi(\rho\beta_T)_s}{(\rho\beta_T)_f}$$

$$a_4 = (1-\varphi) + \frac{\varphi(\rho\beta_C)_s}{(\rho\beta_C)_f}, a_5 = \frac{1}{(1-\varphi)^{2.5}}, a_6 = \frac{a_5}{a_1 Ra}, a_7 = \frac{a_6}{1+\lambda_1}$$

$$a_8 = \frac{a_2}{a_1}, a_9 = \frac{a_3}{a_1}, a_{10} = \frac{a_4}{a_1}, a_{11} = (1-\varphi) + \frac{\varphi(\rho C_p)_s}{(\rho C_p)_f},$$

$$\lambda_f = \frac{k_{nf}}{k_f}, b_o = \frac{Pe a_{11}}{\lambda_f}, b_1 = \frac{Sc}{(1-\varphi)}$$

3. Basic preliminaries

suppose a continuous function $h(t)$, then the Prabhakar fractional derivative ${}^{C}\mathfrak{D}^{\gamma}_{\alpha,\beta,\alpha}$ can be defined as

$${}^{C}\mathfrak{D}^{\gamma}_{\alpha,\beta,\alpha} h(t) = E^{-\gamma}_{\alpha,m-\beta,\alpha} h^m(t) = \int_0^t (t-\tau)^{m-\beta-1} E^{-\gamma}_{\alpha,m-\beta}(\alpha(t-\tau)^{\alpha}) h^m(\tau) d(\tau)$$

Where

$$E^{\gamma}_{\alpha,\beta,\alpha} \mathrm{h}(t) = \int_0^t (t-\tau)^{\beta-1} E^{\gamma}_{\alpha,\beta}(\alpha(t-\tau)^{\alpha}) \mathrm{h}(\tau) d(\tau)$$

Is the Prabhakar integral [40] with its Laplace

Table 3
Numerical analysis of governed profiles at different time.

y	$T_{(y,t)}$ at $t = 0.5$	$T_{(y,t)}$ at $t = 1.0$	$C_{(y,t)}$ at $t = 0.5$	$C_{(y,t)}$ at $t = 1.0$	$V_{(y,t)}$ at $t = 0.5$	$V_{(y,t)}$ at $t = 1.0$
0.1	0.0561	0.0625	0.0561	0.0625	0.2508	0.2720
0.2	0.1146	0.1217	0.1146	0.1271	0.4977	0.5401
0.3	0.1779	0.1959	0.1779	0.1959	0.7355	0.7993
0.4	0.2485	0.2711	0.2485	0.2711	0.9566	1.0425
0.5	0.3294	0.3551	0.3294	0.3551	1.1490	1.2583
0.6	0.4237	0.4506	0.4237	0.4506	1.2935	1.4293
0.7	0.5348	0.5603	0.5348	0.5603	1.3603	1.5281
0.8	0.6664	0.6872	0.6664	0.6872	1.3023	1.5125
0.9	0.8214	0.8372	0.8214	0.8335	1.0464	1.3174

Table 4
The Sherwood number, the Nusselt number, and the skin friction all underwent numerical investigation.

α	Nu at $t = 0.5$	Nu at $t = 1.0$	Sh at $t = 0.5$	Sh at $t = 1.0$	C_f at $t = 0.5$	C_f at $t = 1.0$
0.1	1.2393	1.4339	0.6905	0.7213	1.1905	1.3230
0.2	1.2044	1.3962	0.6843	0.7151	1.1793	1.3100
0.3	1.1703	1.3501	0.6778	0.7070	1.1680	1.2944
0.4	1.1399	1.2982	0.6717	0.6976	1.1577	1.2768
0.5	1.1152	1.2441	0.6664	0.6872	1.1490	1.2583
0.6	1.0739	1.1919	0.6623	0.6769	1.1424	1.2404
0.7	1.0860	1.1451	0.6594	0.6673	1.1380	1.2237
0.8	1.0806	1.1057	0.6579	0.6591	1.1357	1.2098
0.9	1.0802	1.0747	0.6573	0.6524	1.1351	1.1988

$$\mathscr{L}\left\{{}^{C}\mathfrak{D}^{\gamma}_{\alpha,\beta,\alpha} h(t)\right\} = s^{\beta-m}(1-\alpha s^{-\alpha})^{\gamma} \mathscr{L}\{h^m(t)\} \tag{13}$$

As the Prabhakar fractional derivative is based on the comprehensive Fourier also Fick thermal conductivity equations

$$\delta_{(y,t)} = -{}^{C}\mathfrak{D}^{\gamma}_{\alpha,\beta,\alpha} \frac{\partial T_{(y,t)}}{\partial y} \tag{14}$$

$$J_{(y,t)} = -{}^{C}\mathfrak{D}^{\gamma}_{\alpha,\beta,\alpha} \frac{\partial \phi_{(y,t)}}{\partial y} \tag{15}$$

where ${}^{C}\mathfrak{D}^{\gamma}_{\alpha,\beta,\alpha}$ is identified as Prabhakar fractional operator.

4. Solution of governed equations

This framework will be used to carry out the Prabhakar-fractional description-based fractional demonstrating of lead equations and the corresponding fractional model's solution under their respective converted physical conditions.

4.1. Expressions of concentration profile

Numerous methods have been used to solve fractional systems. But in this study, we choose to use the Laplace transformation (L.T.) integral transform strategy by applying L.T. to fractional Eqs. (09) and (15) for the concentration solution profile

$$a_o \quad s \quad \overline{\phi}_{(y,s)} = -\frac{\partial \overline{J}_{(y,s)}}{\partial y} \tag{16}$$

$$\overline{J}_{(y,s)} = -s^{\beta}(1-\alpha s^{-\alpha})^{\gamma} \frac{\partial \overline{\phi}_{(y,s)}}{\partial y} \tag{17}$$

$$\overline{\phi}_{(0,s)} = 0, \overline{\phi}_{(1,s)} = \frac{1}{s}$$

Inserting Eq. (13) into Eq. (12), we get

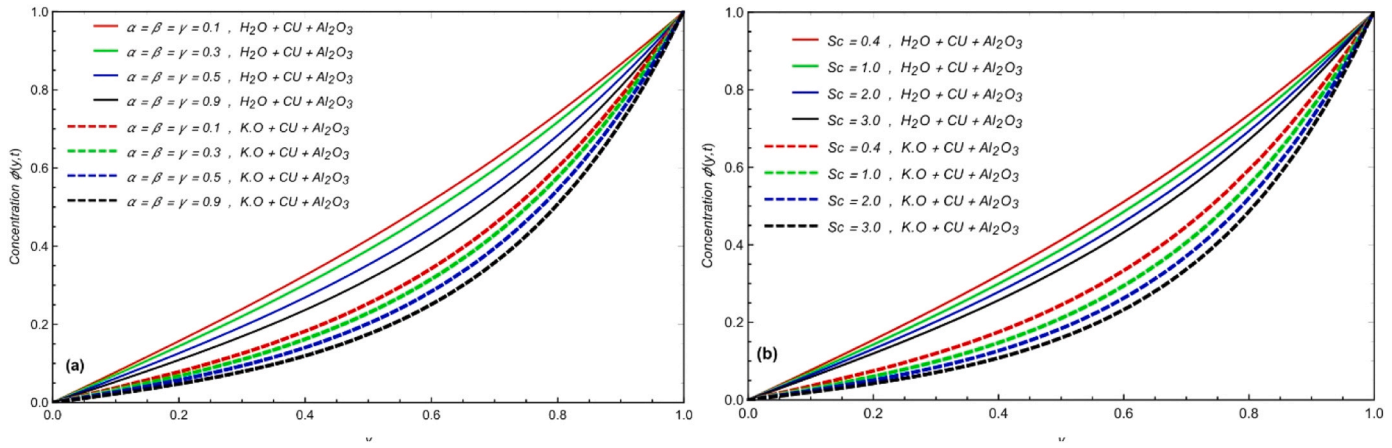

Fig. 2. $C_{(y,t)}$ with variation in fractional parameters and *Sc*.

$$\overline{\phi}_{(y,s)} = \frac{1}{s} \quad \frac{Sinh\left(y\sqrt{\frac{a_1 \quad s^{1-\beta}}{(1-\alpha s^{-\alpha})^{\gamma}}}\right)}{Sinh\left(\sqrt{\frac{a_1 \quad s^{1-\beta}}{(1-\alpha s^{-\alpha})^{\gamma}}}\right)} \tag{18}$$

Stehfest and Tzou's techniques are used in Tables 3–4 to quantitatively evaluate the Laplace inverse of the aforementioned solution.

4.2. Expressions of temperature field

The Laplace technique explains the thermal field for the second-order partial differential equations (08) also (14) and their corresponding values.

$$a_o s \quad \overline{T}_{(y,s)} = -\frac{\partial \overline{\delta}_{(y,s)}}{\partial y} \tag{19}$$

$$\overline{\delta}_{(y,s)} = -s^{\beta}(1-\alpha s^{-\alpha})^{\gamma}\frac{\partial \overline{T}_{(y,s)}}{\partial y} \tag{20}$$

with

$$\overline{T}_{(0,s)} = 0, \left.\frac{\partial \overline{T}_{(y,s)}}{\partial y}\right|_{y=d} = -\left(\frac{1}{s} + \overline{T}_{(1,s)}\right)$$

We get

$$\overline{T}_{(y,s)} = \frac{1}{s\left(\sqrt{\frac{a_o \quad s^{1-\beta}}{(1-\alpha s^{-\alpha})^{\gamma}}} + 1\right)} \quad \frac{Sinh\left(y\sqrt{\frac{a_o \quad s^{1-\beta}}{(1-\alpha s^{-\alpha})^{\gamma}}}\right)}{Sinh\left(\sqrt{\frac{a_o \quad s^{1-\beta}}{(1-\alpha s^{-\alpha})^{\gamma}}}\right)} \tag{21}$$

In Tables 3 and 4, the Laplace inverse of the equation stated above would be statistically investigated.

4.3. Expressions of the velocity field

In the present part, the solution of the flow equation would be derived using the LTE on the second-order PDE Eq. (8). A non-homogeneous differential equation and Eq. (07) are present.

$$a_7(1+\lambda \quad s)\frac{\partial^2 \overline{W}_{(y,s)}}{\partial y^2} - \left(\frac{a_8}{a_7}MSin(\theta) + \frac{a_5}{a_7}K_{eff} + \frac{s}{a_7}\right)\overline{W}_{(y,s)} = -a_8 \quad Gr\overline{T}_{(y,s)} - a_9 \quad Gm \quad \overline{\varphi}_{(y,s)} \tag{22}$$

with conditions

$$\overline{W}_{(0,s)} = 0; \overline{W}_{(d,s)} = F(s)$$

We arrive at the following solution to Eq. (24) by using the matching criteria

$$\begin{aligned}\overline{W}_{(y,s)} = {} & \frac{Sinhy\sqrt{\frac{1}{1+\lambda s}\left(\Re_1 + \Re_2 K_{eff} + \frac{s}{a_7}\right)}}{Sinh\sqrt{\frac{b1}{1+\lambda s}\left(\Re_1 + \Re_2 K_{eff} + \frac{s}{a_7}\right)}}F(s) \\ & + \frac{\Re_3 \quad Gr}{s\left(\sqrt{\frac{a_o \quad s^{1-\beta}}{(1-\alpha s^{-\alpha})^{\gamma}}} + 1\right)} \frac{1}{\frac{a_o \quad s^{1-\beta}}{(1-\alpha s^{-\alpha})^{\gamma}} - \frac{1}{1+\lambda s}\left(\Re_1 + \Re_2 K_{eff} + \frac{s}{a_7}\right)} \\ & \left(\frac{Sinhy\sqrt{\frac{1}{1+\lambda s}\left(\Re_1 + \Re_2 K_{eff} + \frac{s}{a_7}\right)}}{Sinh\sqrt{\frac{b1}{1+\lambda s}\left(\Re_1 + \Re_2 K_{eff} + \frac{s}{a_7}\right)}} - \frac{Sinhy\sqrt{\frac{a_o \quad s^{1-\beta}}{(1-\alpha s^{-\alpha})^{\gamma}}}}{Sinh\sqrt{\frac{a_o \quad s^{1-\beta}}{(1-\alpha s^{-\alpha})^{\gamma}}}}\right) \\ & + \frac{\Re_4 \quad Gm}{s} \frac{1}{\frac{a_1 \quad s^{1-\beta}}{(1-\alpha s^{-\alpha})^{\gamma}} - \frac{1}{1+\lambda s}\left(\Re_1 + \Re_2 K_{eff} + \frac{s}{a_7}\right)} \\ & \left(\frac{Sinhy\sqrt{\frac{1}{1+\lambda s}\left(\Re_1 + \Re_2 K_{eff} + \frac{s}{a_7}\right)}}{Sinh\sqrt{\frac{b1}{1+\lambda s}\left(\Re_1 + \Re_2 K_{eff} + \frac{s}{a_7}\right)}} - \frac{Sinhy\sqrt{\frac{a_1 \quad s^{1-\beta}}{(1-\alpha s^{-\alpha})^{\gamma}}}}{Sinh\sqrt{\frac{a_1 \quad s^{1-\beta}}{(1-\alpha s^{-\alpha})^{\gamma}}}}\right)\end{aligned} \tag{23}$$

$$\Re_1 = \frac{a_8}{a_7}MSin(\theta), \Re_2 = \frac{a_5}{a_7}, \Re_3 = \frac{a_9}{a_7}, \Re_4 = \frac{a_{10}}{a_7}$$

It is challenging to analyze the Laplace inverse of obtained solutions. We likewise utilized numerical methods for the Laplace inverse, namely Stehfest also Tzou's numerical structures, as different writers have used various numerical techniques. These algorithms' mathematical forms [41–43] can be characterized as

$$W(y,t) = \frac{\ln(2)}{t}\sum_{n=1}^{N} v_n \overline{W}\left(y, n\frac{\ln(2)}{t}\right)$$

$$v_n = (-1)^{n+\frac{N}{2}} \sum_{m=\left[\frac{q+1}{2}\right]}^{\min\left(q,\frac{N}{2}\right)} \frac{m^{\frac{N}{2}}(2m)!}{\left(\frac{N}{2}-m\right)!m!(m-1)!(q-m)!(2m-q)!}$$

and

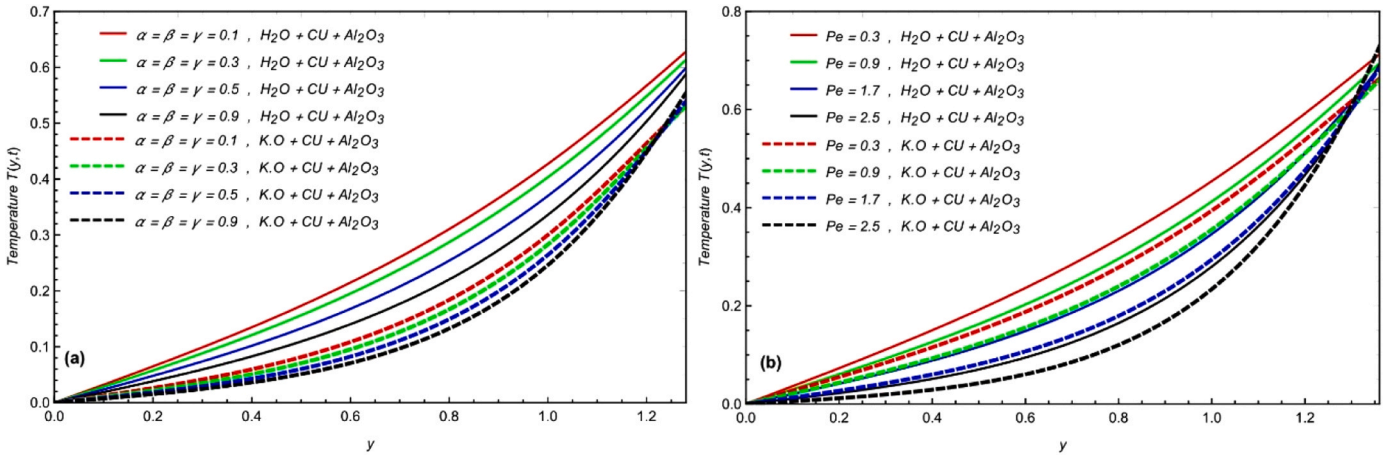

Fig. 3. $T_{(y,t)}$ with variation in fractional parameters and *Pe*.

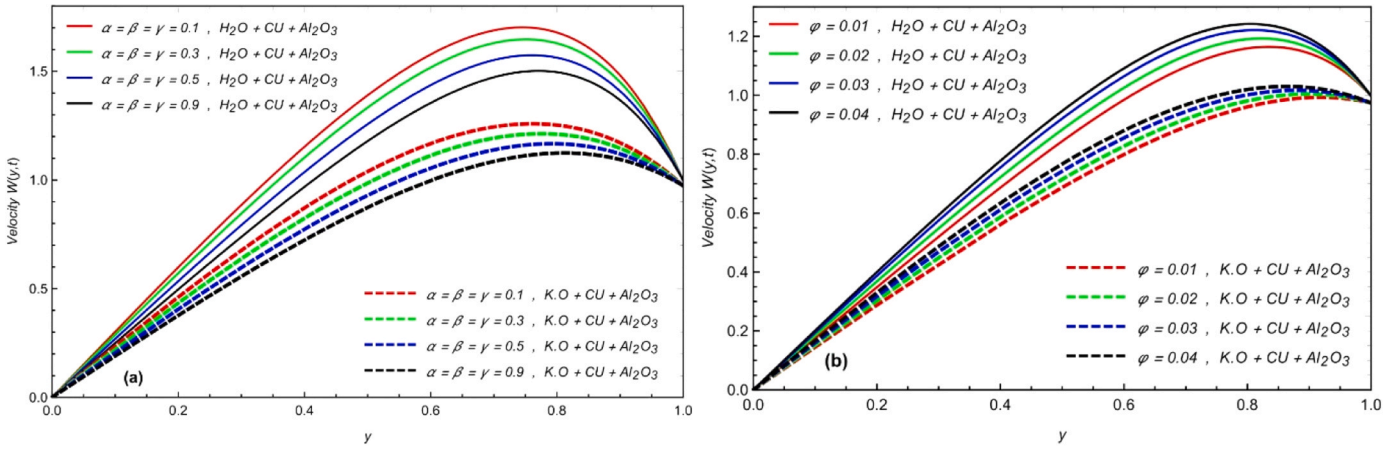

Fig. 4. $W_{(y,t)}$ with variation in α, β, γ and φ with $\alpha, \beta, \gamma = 0.6, Pe = 2.5, Sc = 3.5, M = 1.75, Gr = 1.5, Gm = 2.3, h = 0.5, \varphi = 0.02, K = 1.3, t = 0.8$.

$$W(y,t) = \frac{e^{4.7}}{t}\left[\frac{1}{2}\overline{W}\left(m, \frac{4.7}{t}\right) + \mathrm{Re}\left\{\sum_{j=1}^{N}(-1)^k \overline{W}\left(m, \frac{4.7 + k\pi i}{t}\right)\right\}\right]$$

5. Discussion of results

An investigation is conducted into the numerical interpretation of heat transfer analyses resulting from convection in HNFs made of kerosene oil- and fractionalized water-based materials traveling via a vertical channel. To better comprehend the physical issue, it has been completed. Graphs 2 through 10 illustrate how certain physical parameters, such as the Prabhakar fractional parameters (α, β, γ), Schmidt number *Sc*, Peclet number *Pe*, effective porosity parameter K_{eff}, volume fraction φ, magnetic parameter *M*, thermal Grashof number *Gr*, and mass Grashof number *Gm*, effect on momentum, temperature, and concentration field. Tables 1 & 2 are utilized to summarise the usual thermos-physical properties of base fluids also nanoparticles.

In order to compare different HNFs, including water-Copper-

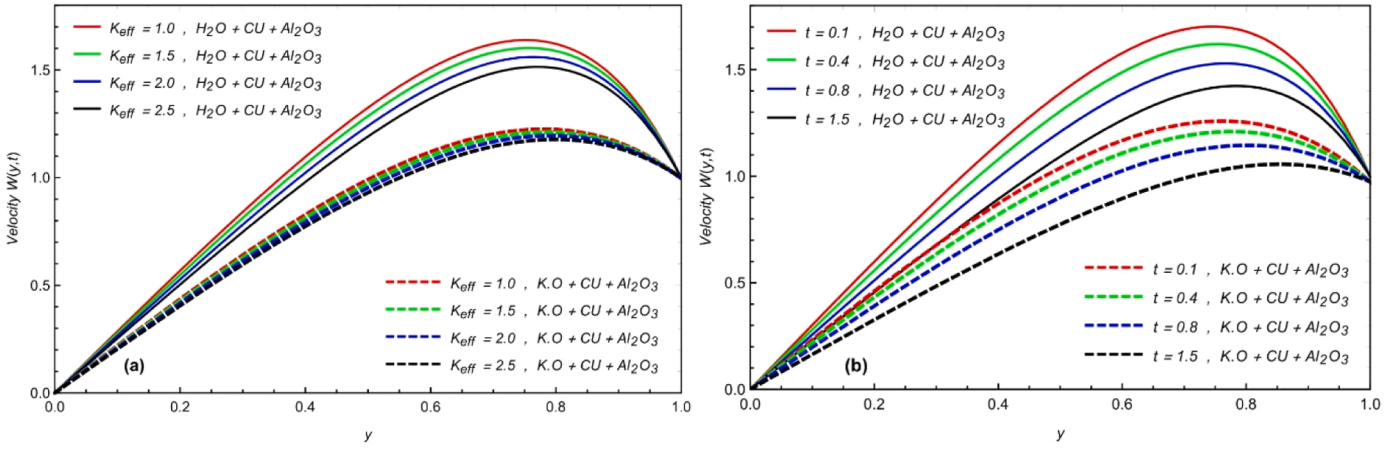

Fig. 5. $W_{(y,t)}$ with variation in K_{eff} and *t* with $\alpha, \beta, \gamma = 0.6, Pe = 2.5, Sc = 3.5, M = 1.75, Gr = 1.5, Gm = 2.3, h\alpha, \beta, \varphi = 0.02, K = 1.3, t = 0.8$.

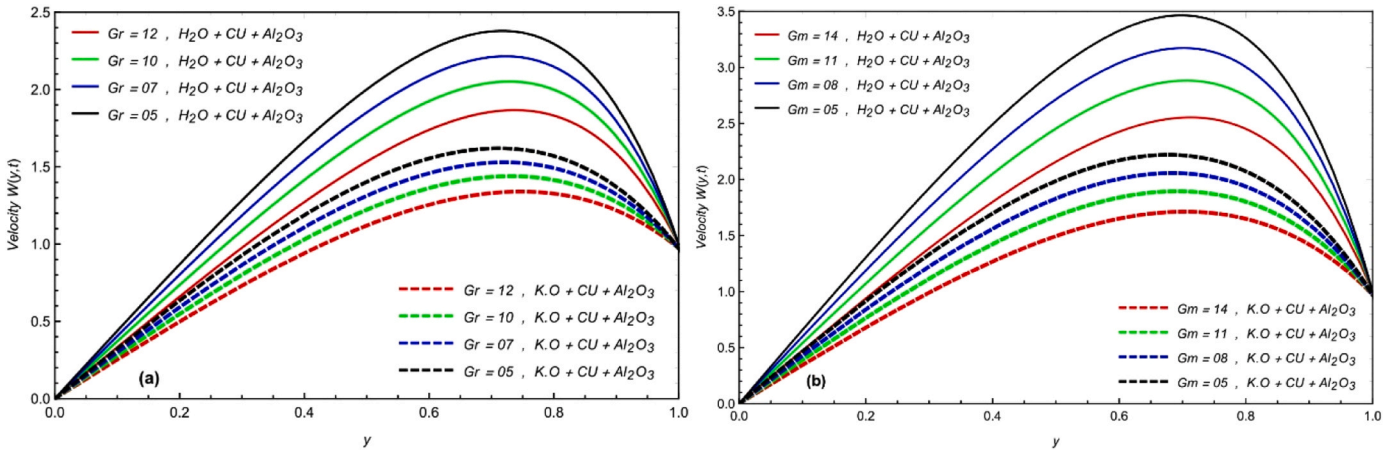

Fig. 6. $W_{(y,t)}$ with variation in Gr and Gm with$\alpha, \beta, \gamma = 0.6, Pe = 2.5, Sc = 3.5, M = 1.75, Gr = 1.5, Gm = 2.3, h\alpha, \beta, \varphi = 0.02, K = 1.3, t = 0.8$.

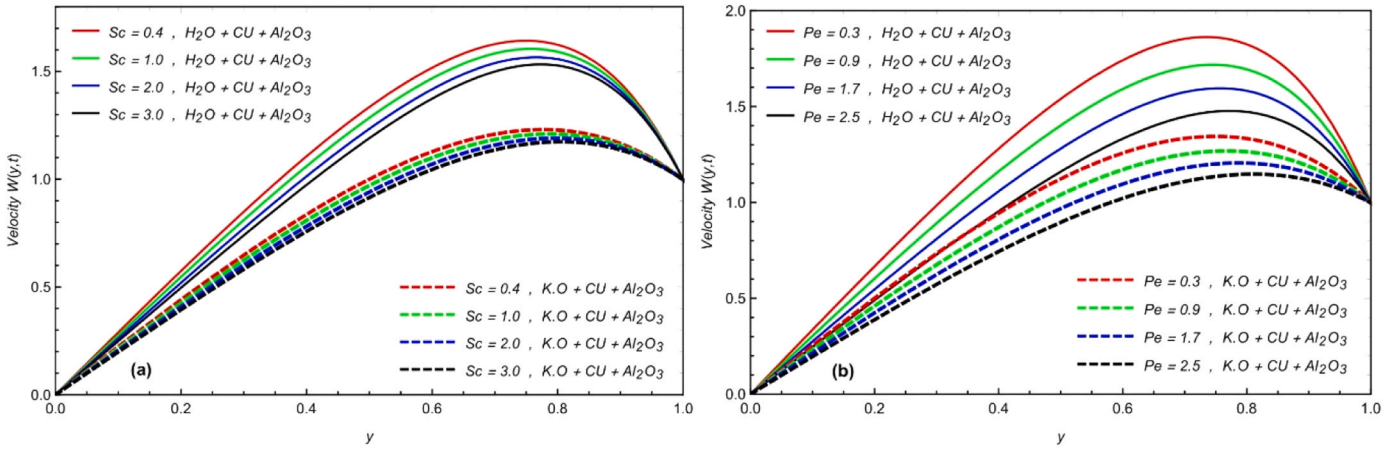

Fig. 7. $W_{(y,t)}$ with variation in Sc and Pe with$\alpha, \beta, \gamma = 0.6, Pe = 2.5, Sc = 3.5, M = 1.75, Gr = 1.5, Gm = 2.3, h\alpha, \beta, \varphi = 0.02, K = 1.3, t = 0.8$.

Aluminum Oxide ($H_2O - Cu - Al_2O_3$) and kerosene oil-Copper-Aluminum Oxide ($K.O - Cu - Al_2O_3$), we designed Fig. 2a and b for various values of fractional parameters (, and) and Schmidt number Sc on the concentration profile. It is apparent from these figures that the concentration profile is reduced by considering larger values of fractional parameters and Schmidt number, respectively. The fractional parameters may help control the concentration boundary layer. The effect of Sc is due to the decreasing in the boundary layer of concentration that occurred as we boost the Schmidt number. Besides, the development in concentration rate due to ($H_2O - Cu - Al_2O_3$) is more progressive than (KO $- Cu - Al_2O_3$), because of the physical characteristics of specific nanoparticles. The impacts of fractional parameters and Peclet number Pe on the temperature profile, along with the comparison of different HNFs that are ($H_2O - Cu - Al_2O_3$) and (KO $- Cu - Al_2O_3$) are displayed in Fig. 3a and b. It is clear from these figures that larger values of fractional parameters also Peclet number, respectively, decline the thermal profile. The fractional parameters may also help control the thermal boundary layer. Further, the development in the thermal profile is due to ($H_2O - Cu - Al_2O_3$) is more progressive in this case than (KO $- Cu - Al_2O_3$), because of the physical characteristics of specific nanoparticles. We designed Fig. 4a and b for different values of fractional parameters (α, β, and γ) and volume fraction φ on the momentum profile, along with the evaluation of dissimilar HNFs that are ($H_2O - Cu - Al_2O_3$) and (KO $- Cu - Al_2O_3$). It is evident from Fig. 4a that the momentum profile declined through larger values of fractional parameters. The fractional parameters may help control the momentum boundary layer. The result of φ is declining on the momentum profile with increasing values of φ. Physically, for great values, viscous forces dominate, and velocity declines. Besides, the development in velocity rate due to ($H_2O - Cu - Al_2O_3$) is more progressive than (KO $- Cu - Al_2O_3$), because of the physical characteristics of specific nanoparticles.

The impacts of effective porosity parameter K_{eff} and time values t on the velocity profile, along with the comparison of different HNFs that are ($H_2O - Cu - Al_2O_3$) and (KO $- Cu - Al_2O_3$) are displayed in Fig. 5a and b. It is clear from these figures that the velocity profile is declined by larger values of fractional parameters and time values, respectively. Further, the development in velocity profile is due to ($H_2O - Cu - Al_2O_3$) is more enlarged than (KO $- Cu - Al_2O_3$), due to the physical characteristics of specific nanoparticles. Furthermore, by growing the value of K_{eff}, the holes are suggestively adequate, and thus the porosity resistance declined. Consequently, the velocity rises as the presence of the porous surface advance the resistance to the fluid.

Fig. 6a shows that velocity increases as we raise the values of Gr. Physically, when Gr is enlarged, the effect of buoyant forces becomes more vigorous, which marks more convection. So, the velocity rises. Fig. 6b shows that a parallel trend is perceived for Gm. As Gm is the ratio of viscous forces to buoyant forces due to concentration difference, increasing the value of Gm raises fluid velocity and thickness of the boundary layer in both situations. Fig. 6a and b show that the development in velocity profile is due to ($H_2O - Cu - Al_2O_3$) is more progressive than (KO $- Cu - Al_2O_3$), due to the physical characteristics of specific nanoparticles.

We intended Fig. 7a and b to compare two HNFs, namely (H_2O –

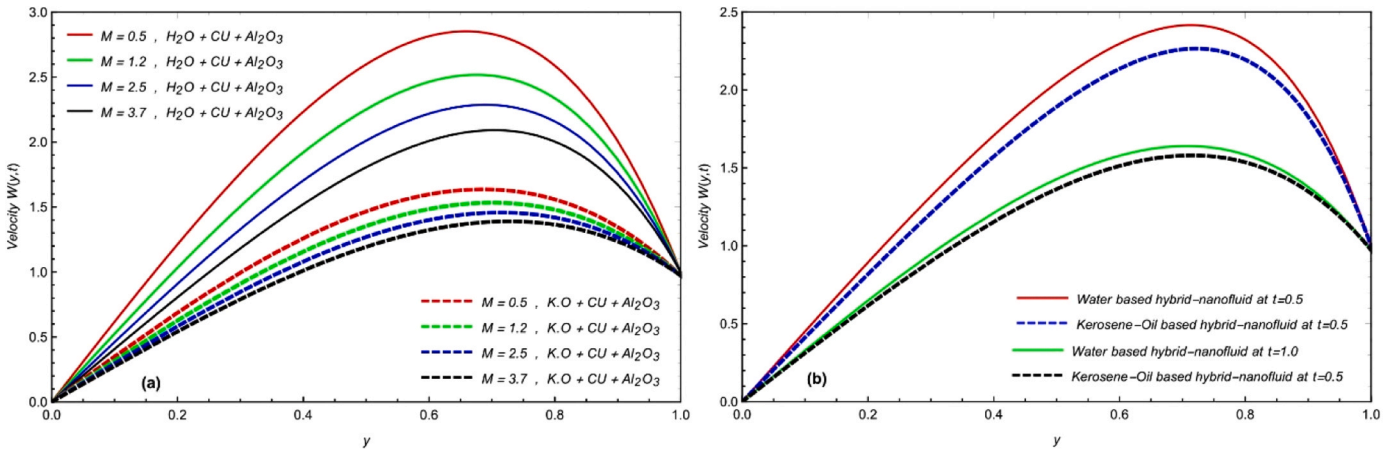

Fig. 8. $W_{(y,t)}$ with variation in M and comparison of different considered fluids.

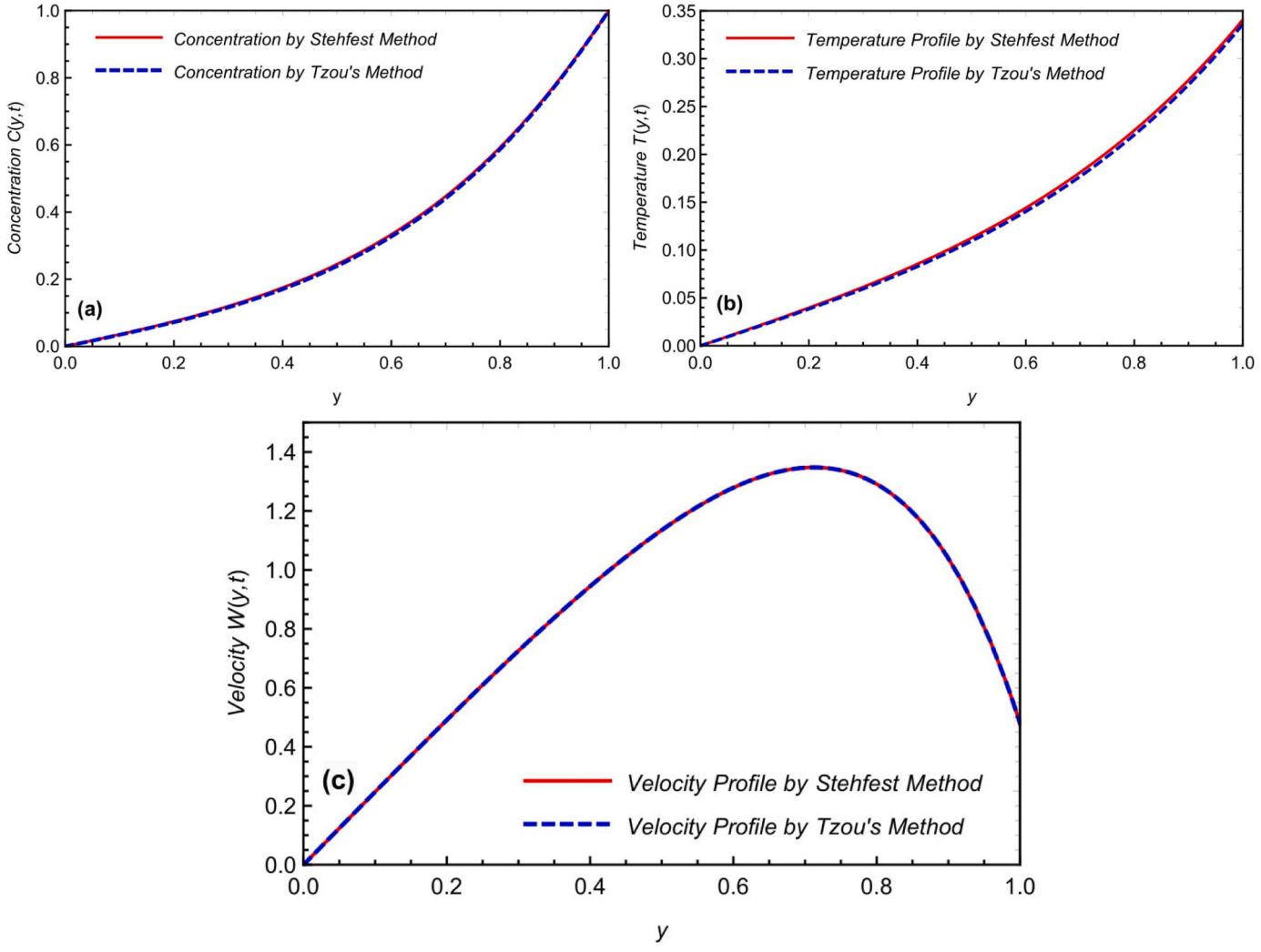

Fig. 9. Comparison of numerical schemes of governed equations.

$Cu - Al_2O_3$) and ($K.O - Cu - Al_2O_3$), as well as different values of Schmidt number *Sc* and Peclet number *Pe* on the velocity profile. These numbers make it clear that taking bigger values of Sc and Pe into account reduces velocity. The effect of Sc is a result of the boundary layer of concentration becoming less concentrated as the Schmidt number increased. Additionally, due to the physical properties of some nanoparticles, the development in velocity rate caused by ($H_2O - Cu - Al_2O_3$) is more progressive than ($K.O - Cu - Al_2O_3$).

Multiple HNFs are compared in Fig. 8a, which demonstrates how the velocity falls off as M rises. Physically, it might retaliate against the drag

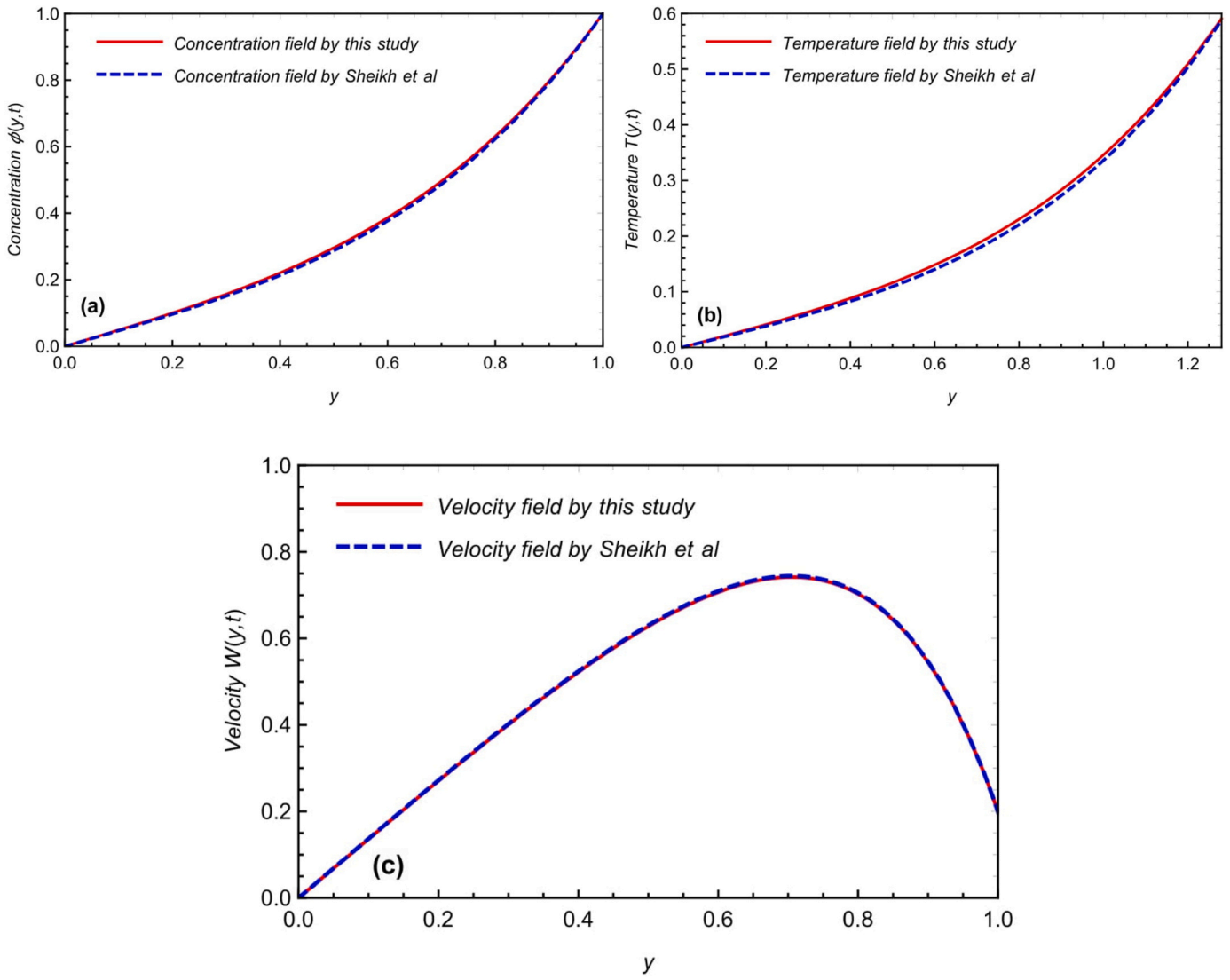

Fig. 10. Comparison of velocity, concentration, and temperature field with Sheikh et al. [44].

Table 5
Numerical analysis of Numerical algorithms at different time.

y	$T_{(y,t)}$ by Stehfest at $t = 0.5$	$T_{(y,t)}$ by Tzou's at $t = 1.0$	$C_{(y,t)}$ by Stehfest at $t = 0.5$	$C_{(y,t)}$ by Tzou's at $t = 1.0$	$V_{(y,t)}$ by Stehfest at $t = 0.5$	$V_{(y,t)}$ by Tzou's at $t = 1.0$
0.1	0.0608	0.0610	0.0608	0.0609	0.5626	0.2659
0.2	0.1237	0.1241	0.1237	0.1239	0.5272	0.5280
0.3	0.1910	0.1916	0.1910	0.1913	0.7798	0.7809
0.4	0.2650	0.2658	0.2650	0.2654 0.3468	1.0160	1.0175
0.5	0.3482	0.3491	0.3482	0.3486	1.2241	1.2261
0.6	0.4434	0.4443	0.4434	0.4439	1.3861	1.3886
0.7	0.5536	0.5544	0.5536	0.5540	1.4738	1.4769
0.8	0.6818	0.6825	0.6818	0.6821	1.4430	1.4468
0.9	0.8304	0.8308	0.8304	0.8306	1.2250	1.2309

force, which modifies the fluid motion's velocity. Velocity falls as a result. Fig. 8b shows that the effects of both HNFs are amplified more in a brief period of time $(t = 0.5)$ than over a longer period of time $(t = 1.0)$. Fig. 9a, b, and c compare the Stehfest and Tzou numerical systems for all profiles. The validity of the present investigation is based on the relevance of many profile curves overlapping. In light of the concentration, temperature, and momentum findings from Sheikh et al. [44], Fig. 10a, b, and c were made to evaluate the validity of our findings. By superimposing the two curves, these graphs enable us to conclude that the results we have gotten are consistent with those suggested by Sheikh et al. [44]. The Nusselt number, Sherwood number, and skin friction are used in Tables 3–5 to compare leading equations using different numerical techniques.

6. Conclusions

With water and kerosene oil as the base fluid, the free convective flow of unstable also compact flow mixed with (Cu, Al_2O_3) nanofluid is investigated by passing through two parallel poured plates. Using the Laplace transformation, a fractional model is created using the utmost current definition of a fractional derivative, the Prabhakar fractional derivative. Graphical analysis shows the effects of various limitations on the temperature, concentration, and momentum profile values obtained. The following are some definitive conclusions from this investigation in bullet form:

- This technique might be widened to include more changed physical sciences classes with intricate geometries.
- The upgrading value of *Pr* slow down both momentum also thermal profiles.

- The concentration field grows by decreasing the value of fractional restraints.
- The momentum profile is upgraded by the parameters Gr, Gm whereas declarations are because of M and Sc.
- By adjusting the fractional parameter, one can manipulate the thickness of the momentum and thermal boundary layers.
- The solutions found through the study can help with the precise interpretation of empirical data and enable the testing of various solution approximations as required.
- The findings of this investigation are supported by both the numerical scheme's results and the data presented in Sheikh et al.'s research [44]. The interchange of the curves further confirms the conclusions.

The recommendations that follow are meant to suggest a future extension of the problem that this study looks at and are based on techniques, expansions, geometries, and analyses. To evaluate the current situation, a horizontal plate with a fixed length and linear velocity might be utilized. It is also possible to analyses the same problem using a Keller Box technique.

Declaration of Competing Interest

The authors declare that they have no known competing financial interests or personal relationships that could have appeared to influence the work reported in this paper.

Acknowledgement

The authors thank the Deanship of Scientific Research at King Khalid University for funding this work through a large group research project under Grant number RGP 2/554/44.

References

[1] F. Bräuer, E. Trautner, J. Hasslberger, P. Cifani, M. Klein, Turbulent Bubble-Laden channel flow of power-law fluids: a direct numerical simulation study, Fluids vol. 6 (2021) 40.
[2] Y. Zheng, H. Yang, H. Mazaheri, A. Aghaei, N. Mokhtari, M. Afrand, "An investigation on the influence of the shape of the vortex generator on fluid flow and turbulent heat transfer of hybrid nanofluid in a channel,", J. Therm. Anal. Calorim. vol. 143 (2021) 1425–1438.
[3] A. D'Ippolito, F. Calomino, G. Alfonsi, A. Lauria, "Flow resistance in open channel due to vegetation at reach scale: a review,", Water vol. 13 (2021) 116.
[4] S.U. Choi, J.A. Eastman, Enhancing Thermal Conductivity of Fluids with Nanoparticles, Argonne National Lab.(ANL),, Argonne, IL (United States), 1995.
[5] S. Nadeem, S. Ahmad, M.N. Khan, "Mixed convection flow of hybrid nanoparticle along a Riga surface with Thomson and Troian slip condition,", J. Therm. Anal. Calorim. vol. 143 (2021) 2099–2109.
[6] M. Reddy, S. Shehzad, "Molybdenum disulfide and magnesium oxide nanoparticle performance on micropolar Cattaneo-Christov heat flux model,", Appl. Math. Mech. vol. 42 (2021) 541–552.
[7] I. Wole-Osho, E.C. Okonkwo, H. Adun, D. Kavaz, S. Abbasoglu, "An intelligent approach to predicting the effect of nanoparticle mixture ratio, concentration and temperature on thermal conductivity of hybrid nanofluids,", J. Therm. Anal. Calorim. vol. 144 (2021) 671–688.
[8] M.E. Haque, M.S. Hossain, H.M. Ali, "Laminar forced convection heat transfer of nanofluids inside non-circular ducts: A review,", Powder Technol. vol. 378 (2021) 808–830.
[9] N.S. Khashi'ie, N. Md Arifin, I. Pop, R. Nazar, "Melting heat transfer in hybrid nanofluid flow along a moving surface,", J. Therm. Anal. Calorim. (2020) 1–12.
[10] A. Shahsavar Goldanlou, M. Sepehrirad, M. Papi, A.K. Hussein, M. Afrand, S. Rostami, "Heat transfer of hybrid nanofluid in a shell and tube heat exchanger equipped with blade-shape turbulators,", J. Therm. Anal. Calorim. vol. 143 (2021) 1689–1700.
[11] E. Montazer, M.B. Shafii, E. Salami, M.R. Muhamad, H. Yarmand, S. Gharehkhani, et al., "Heat transfer in turbulent nanofluids: Separation flow studies and development of novel correlations,", Adv. Powder Technol. vol. 31 (2020) 3120–3133.
[12] A. Raza, R. Ali, S.M. Eldin, S.H. Alfalqui, A.H. Ali, "New fractional approach for CMC and water based hybrid nanofluid with slip boundary layer: Applications of fractal fractional derivative,", Case Stud. Therm. Eng. (2023), 103280.
[13] B. Ahmad, S. Bibi, S.U. Khan, T. Abbas, A. Raza, "Bioconvective thermal transport of micropolar nanofluid with applications of viscous dissipation and micro-rotational features,", Waves Random Complex Media (2023) 1–19.
[14] A. Raza, S.U. Khan, T. Thumma, A.U. Haq, "Fractional simulations for slip flow of Casson CMC-CNTs hybrid nanofluid with Mittag-Leffler kernel and Prabhakar fractional simulations,", Waves Random Complex Media (2023) 1–17.
[15] M. Benkhedda, T. Boufendi, T. Tayebi, A.J. Chamkha, "Convective heat transfer performance of hybrid nanofluid in a horizontal pipe considering nanoparticles shapes effect,", J. Therm. Anal. Calorim. vol. 140 (2020) 411–425.
[16] A. Bhattad, J. Sarkar, P. Ghosh, "Hydrothermal performance of different alumina hybrid nanofluid types in plate heat exchanger,", J. Therm. Anal. Calorim. vol. 139 (2020) 3777–3787.
[17] M. Izadi, "Effects of porous material on transient natural convection heat transfer of nano-fluids inside a triangular chamber,", Chin. J. Chem. Eng. vol. 28 (2020) 1203–1213.
[18] I. Waini, A. Ishak, T. Groşan, I. Pop, "Mixed convection of a hybrid nanofluid flow along a vertical surface embedded in a porous medium,", Int. Commun. Heat. Mass Transf. vol. 114 (2020), 104565.
[19] N.S. Pandya, A.N. Desai, A.K. Tiwari, Z. Said, "Influence of the geometrical parameters and particle concentration levels of hybrid nanofluid on the thermal performance of axial grooved heat pipe,", Therm. Sci. Eng. Prog. vol. 21 (2021), 100762.
[20] H. Babazadeh, Z. Shah, I. Ullah, P. Kumam, A. Shafee, "Analysis of hybrid nanofluid behavior within a porous cavity including Lorentz forces and radiation impacts,", J. Therm. Anal. Calorim. vol. 143 (2021) 1129–1137.
[21] A. Asadi, I.M. Alarifi, L.K. Foong, "An experimental study on characterization, stability and dynamic viscosity of CuO-TiO2/water hybrid nanofluid,", J. Mol. Liq. vol. 307 (2020), 112987.
[22] M. Danish Ikram, M. Imran Asjad, A. Ahmadian, M. Ferrara, "A new fractional mathematical model of extraction nanofluids using clay nanoparticles for different based fluids,", Math. Methods Appl. Sci. (2020).
[23] G. Huminic, A. Huminic, "Entropy generation of nanofluid and hybrid nanofluid flow in thermal systems: a review,", J. Mol. Liq. vol. 302 (2020), 112533.
[24] S. Nadeem, N. Abbas, M. Malik, "Inspection of hybrid based nanofluid flow over a curved surface,", Comput. Methods Prog. Biomed. vol. 189 (2020), 105193.
[25] K. Zheng, A. Raza, A.M. Abed, H. Khursheed, L.F. Seddek, A.H. Ali, et al., New fractional approach for the simulation of (Ag) and (TiO2) mixed hybrid nanofluid flowing through a channel: Fractal fractional derivative, Case Stud. Therm. Eng. vol. 45 (2023), 102948.
[26] Q. Ali, M. Amir, A. Raza, U. Khan, S.M. Eldin, A.M. Alotaibi, et al., "Thermal investigation into the Oldroyd-B hybrid nanofluid with the slip and Newtonian heating effect: Atangana–Baleanu fractional simulation,", Front. Mater. vol. 10 (2023) 1114665.
[27] S.U. Khan, A. Raza, A. Kanwal, "The inclined surface flow of hybrid nanofluid with Newtonian heating and general velocity flow constraints: the Prabhakar model,", Waves Random Complex Media (2022) 1–12.
[28] A. Raza, U. Khan, A. Zaib, W. Weera, A.M. Galal, "A comparative study for fractional simulations of Casson nanofluid flow with sinusoidal and slipping boundary conditions via a fractional approach,", AIMS Math. vol. 7 (2022) 19954–19974.
[29] N.A. Shah, A.A. Zafar, S. Akhtar, "General solution for MHD-free convection flow over a vertical plate with ramped wall temperature and chemical reaction,", Arab. J. Math. vol. 7 (2018) 49–60.
[30] Q. Ali, S. Riaz, A.U. Awan, K.A. Abro, "Thermal investigation for electrified convection flow of Newtonian fluid subjected to damped thermal flux on a permeable medium,", Phys. Scr. vol. 95 (2020), 115003.
[31] A. Raza, U. Khan, S.M. Eldin, A.M. Alotaibi, S. Elattar, B.C. Prasannakumara, et al., "Significance of Free Convection Flow over an Oscillating Inclined Plate Induced by Nanofluid with Porous Medium: The Case of the Prabhakar Fractional Approach,", Micromachines vol. 13 (2022) 2019.
[32] A. Raza, U. Khan, Z. Raizah, S.M. Eldin, A.M. Alotaibi, S. Elattar, et al., "Numerical and Computational Analysis of Magnetohydrodynamics over an Inclined Plate Induced by Nanofluid with Newtonian Heating via Fractional Approach,", Symmetry vol. 14 (2022) 2412.
[33] J. Hristov, "Integral solutions to transient nonlinear heat (mass) diffusion with a power-law diffusivity: a semi-infinite medium with fixed boundary conditions,", Heat. Mass Transf. vol. 52 (2016) 635–655.
[34] N. Ahmed, N. Ali Shah, B. Ahmad, S.I. Shah, S. Ulhaq, M.R. Gorji, "Transient MHD convective flow of fractional nanofluid between vertical plates,", J. Appl. Comput. Mech. vol. 5 (2019) 592–602.
[35] R. Garra, R. Garrappa, "The Prabhakar or three parameter Mittag–Leffler function: Theory and application,", Commun. Nonlinear Sci. Numer. Simul. vol. 56 (2018) 314–329.
[36] A. Giusti, I. Colombaro, "Prabhakar-like fractional viscoelasticity,", Commun. Nonlinear Sci. Numer. Simul. vol. 56 (2018) 138–143.
[37] P. Mayeli, G.J. Sheard, "Buoyancy-driven flows beyond the Boussinesq approximation: A brief review,", Int. Commun. Heat. Mass Transf. vol. 125 (2021), 105316.
[38] Y.M. Chu, S. Bilal, M.R. Hajizadeh, "Hybrid ferrofluid along with MWCNT for augmentation of thermal behavior of fluid during natural convection in a cavity,", Math. Methods Appl. Sci. (2020).
[39] S. Sarwar, M. Aleem, M.I. Asjad, T. Muhammad, Fractional study for transient free convection flow in a channel with Mittag-Leffler memory, Math. Probl. Eng. vol. 2022 (2022).
[40] J. Zhang, A. Raza, U. Khan, Q. Ali, A. Zaib, W. Weera, et al., "Thermophysical study of oldroyd-b hybrid nanofluid with sinusoidal conditions and permeability: a Prabhakar fractional approach,", Fractal Fract. vol. 6 (2022) 357.
[41] A. Raza, S.U. Khan, M.I. Khan, S. Farid, T. Muhammad, M.I. Khan, et al., Fractional order simulations for the thermal determination of graphene oxide (GO) and

molybdenum disulphide (MoS2) nanoparticles with slip effects, Case Stud. Therm. Eng. vol. 28 (2021), 101453.

[42] A. Raza, I. Khan, S. Farid, C.A. My, A. Khan, H. Alotaibi, "Non-singular fractional approach for natural convection nanofluid with Damped thermal analysis and radiation,", Case Stud. Therm. Eng. vol. 28 (2021), 101373.

[43] B. Guo, A. Raza, K. Al-Khaled, S.U. Khan, S. Farid, Y. Wang, et al., "Fractional-order simulations for heat and mass transfer analysis confined by elliptic inclined plate with slip effects: A comparative fractional analysis,", Case Stud. Therm. Eng. vol. 28 (2021), 101359.

[44] N.A. Sheikh, D.L. Chuan Ching, I. Khan, A. Ahmad, S. Ammad, "Concrete based Jeffrey nanofluid containing zinc oxide nanostructures: application in cement industry,", Symmetry vol. 12 (2020) 1037.